

# Microbial manganese(III) reduction fuelled by anaerobic acetate oxidation

Nadia Szeinbaum,<sup>1</sup> Hui Lin,<sup>2</sup> Jay A. Brandes,<sup>3</sup>  
Martial Taillefert,<sup>2</sup> Jennifer B. Glass<sup>2</sup> and  
Thomas J. DiChristina<sup>1\*</sup>

<sup>1</sup>*School of Biology, Georgia Institute of Technology, Atlanta, GA, USA.*

<sup>2</sup>*School of Earth and Atmospheric Sciences, Georgia Institute of Technology, Atlanta, GA, USA.*

<sup>3</sup>*Skidaway Institute of Oceanography, Savannah, GA, USA.*

## Summary

**Soluble manganese in the intermediate +III oxidation state ( $\text{Mn}^{3+}$ ) is a newly identified oxidant in anoxic environments, whereas acetate is a naturally abundant substrate that fuels microbial activity. Microbial populations coupling anaerobic acetate oxidation to  $\text{Mn}^{3+}$  reduction, however, have yet to be identified. We isolated a *Shewanella* strain capable of oxidizing acetate anaerobically with  $\text{Mn}^{3+}$  as the electron acceptor, and confirmed this phenotype in other strains. This metabolic connection between acetate and soluble  $\text{Mn}^{3+}$  represents a new biogeochemical link between carbon and manganese cycles. Genomic analyses uncovered four distinct genes that allow for pathway variations in the complete dehydrogenase-driven TCA cycle that could support anaerobic acetate oxidation coupled to metal reduction in *Shewanella* and other Gammaproteobacteria. An oxygen-tolerant TCA cycle supporting anaerobic manganese reduction is thus a new connection in the manganese-driven carbon cycle, and a new variable for models that use manganese as a proxy to infer oxygenation events on early Earth.**

## Introduction

Microbial Mn cycling in marine and freshwater environments is generally assumed to consist of  $\text{Mn}^{2+}$  oxidation to solid Mn(IV) oxides in oxic aquatic

environments and Mn(IV) reduction to  $\text{Mn}^{2+}$  in anoxic ecosystems (Post, 1999; Lovley, 2013; Vandieken and Thamdrup, 2014). Thus, field- and laboratory-based studies of microbial Mn reduction have focused largely on Mn(IV)-driven pathways. This dogma was recently overturned with the finding that soluble  $\text{Mn}^{3+}$  can dominate the soluble Mn pool at  $\mu\text{M}$  concentrations in sediment pore waters (Trouwborst *et al.*, 2006; Madison *et al.*, 2011; 2013) and water columns (Trouwborst *et al.*, 2006; Schnetger and Dellwig, 2012; Luther III *et al.*, 2015; Oldham *et al.*, 2015) in marine environments. Soluble  $\text{Mn}^{3+}$  may form abiotically by Mn(IV) reductive dissolution of Mn(IV) oxides by siderophore-like ligands (Duckworth and Sposito, 2005; 2007) or during microbial  $\text{Mn}^{2+}$  oxidation (Tebo *et al.*, 2005; Webb *et al.*, 2005) or Mn(IV) reduction (Hui *et al.*, 2012). The resulting Mn can persist in solution stabilized by organic (Oldham *et al.*, 2017) or inorganic (Yakushev *et al.*, 2009) ligands. Although  $\text{Mn}^{3+}$  is soluble, electron transport and protein secretion pathways involved in extracellular metal reduction are required for electron transfer to  $\text{Mn}^{3+}$  (Szeinbaum *et al.*, 2014). Therefore,  $\text{Mn}^{3+}$  has the potential to act as an important soluble extracellular electron acceptor fuelling heterotrophs under anoxic conditions.

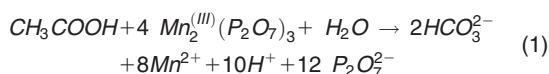
Acetate is one of the most abundant volatile fatty acids fuelling manganese reduction in aquatic environments (Vandieken *et al.*, 2012; 2014) and is also one of the primordial organic carbon substrates for microbial life (Russell and Martin, 2004). In anoxic sediments, acetate is one of the most abundant short chain fatty acids, (typically 0.01 to 1 mM) (Blair *et al.*, 1991; de Graaf *et al.*, 1996; Finke *et al.* 2007). Acetate can be produced via biotic or abiotic processes or imported from thermophilic ecological processes (Balba and Nedwell, 1982; Tor *et al.*, 2001; Heuer *et al.* 2009; Ferry 2015). Acetate-producing microorganisms include acetogenic autotrophs that produce acetate via the Wood-Ljungdahl Pathway (WLP) (Ragsdale and Pierce, 2008) or acetogenic heterotrophs that produce acetate during incomplete oxidation of fermentation products (Lovley, 2008).

The prevalence of acetate in marine and freshwater sediments has resulted in a wealth of biogeochemical

Received 17 March, 2017; accepted 13 June, 2017. \*For correspondence. E-mail Thomas.dichristina@biology.gatech.edu; Tel. 404-894-8419; Fax 404-385-4440.

studies on anaerobic acetate metabolism under sulphate-reducing and methanogenic conditions, yet outside two members of the *Geobacter* family, little is known about anaerobic acetate metabolism under metal-reducing conditions (Lovley *et al.*, 2004; Finke *et al.*, 2007; Lovley, 2008; Elifantz *et al.*, 2010; Vandieken *et al.*, 2012; 2013; 2014). *Geobacter* and *Shewanella* are model dissimilatory metal-reducing microbes distinguished not only by differences in the biochemical pathway for extracellular metal-reduction but also by the apparent inability of the *Shewanella* genus to oxidize acetate coupled to metal reduction, which *Geobacter* carries out readily (Bird *et al.*, 2011; Lovley, 2013).

Redox potentials of acetate (−290 mV) and Mn(III) (430 mV) (Kostka *et al.*, 1995) at circumneutral pH suggest that anaerobic oxidation of acetate coupled to  $\text{Mn}^{3+}$  could support microorganisms in suboxic environments. The anaerobic oxidation of acetate coupled to  $\text{Mn}^{3+}$ -pyrophosphate reduction is described by the following overall stoichiometry (Eq. (1)):



Here, we show that  $\text{Mn}^{3+}$  can act as an electron acceptor during acetate oxidation in anoxic enrichment cultures from a coastal salt marsh, dominated by *Shewanella*. We confirm this phenotype in *Shewanella* isolates from our enrichment and related strains, thus expanding the ecological niche of *Shewanella* to include anaerobic acetate oxidation with metal reduction, and show that  $\text{Mn}^{3+}$  can support microbial metabolism.

## Results and discussion

### Distribution of the main redox species in salt marsh sediments

Sediment depth profiles of the main redox species in creek bank sediments resemble previously obtained data in this environment (Taillefert *et al.*, 2007; Hui and Taillefert, 2014). Dissolved oxygen was consumed within a couple of millimetres from the sediment-water interface,  $\text{Mn}^{2+}$  increased from immediately suboxic reached a maximum at  $\sim 140 \mu\text{M}$  in the first 20 mm, and decreased below detection limit by 60 mm (Fig. 1A left panel). As expected from thermodynamic considerations (Froelich *et al.*, 1979), the onset of Fe(III) reduction was located below the  $\text{Mn}^{2+}$  production zone (45 mm), and  $\text{Fe}^{2+}$  reached concentrations as high as  $600 \mu\text{M}$  at 65 mm then gradually decreasing with depth. Soluble organic-Fe(III) complexes, hypothesized to be produced during microbial Fe(III) reduction (Beckler *et al.*, 2015), mirrored the  $\text{Fe}^{2+}$  profile, reached current intensities as high as 400 nA around 90 mm, then remained constant

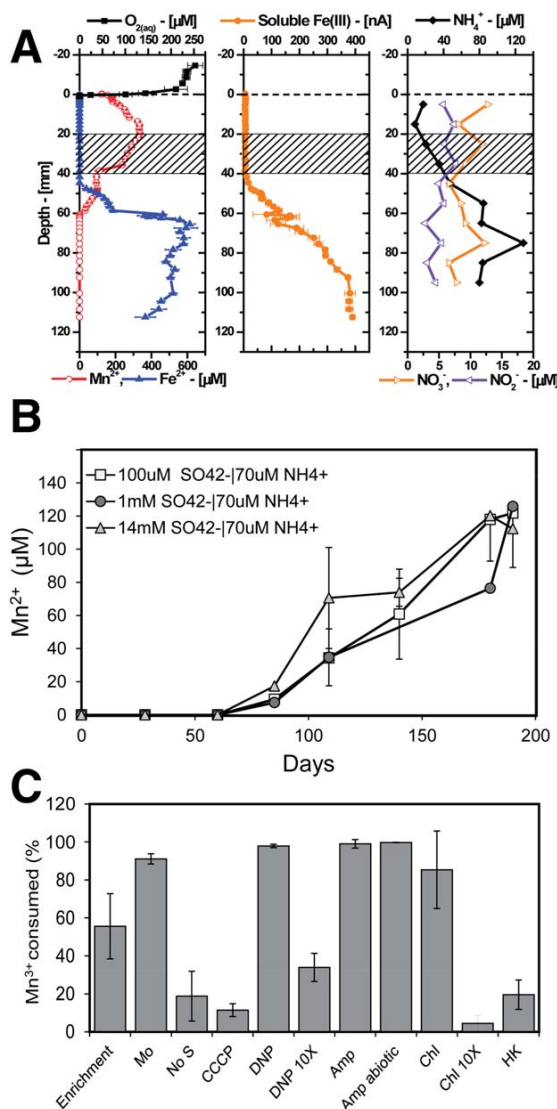


**Fig. 1.**  $\text{Mn}^{3+}$  reduction activity of the enrichment culture (year 2) from SKIO.

A. Electron acceptor depth profiles of sediment core samples used for inoculum. Highlighted in grey dashed boxes is the 20–40 mm zone below the sediment-water interphase selected for inoculation. B.  $\text{Mn}^{2+}$  production by sediment-free  $\text{Mn}^{3+}$ -reducing enrichment culture amended with 200  $\mu\text{M}$  acetate and 0.1, 1, or 14 mM  $\text{SO}_4^{2-}$ , indicating that sulfate-reducing bacteria were not involved. C. Extent of  $\text{Mn}^{3+}$  reduction of the enrichment culture incubated for 60 days under anoxic conditions and amended with sodium molybdate (Mo), 140 mM; sulphate-free (No S) (10  $\mu\text{M}$  for assimilation); carbonyl cyanide m-chlorophenyl hydrazone (CCCP), 200  $\mu\text{M}$ ; dinitrophenol (DNP), 360 and 3600  $\mu\text{M}$ ; ampicillin (Amp), 2.3 mM; chloramphenicol (Chl), 62 and 620  $\mu\text{M}$ ; or heat killed (HK). [Colour figure can be viewed at [wileyonlinelibrary.com](http://wileyonlinelibrary.com)]

throughout the rest of the measured depths (Fig. 1A middle panel). Concentrations of nitrite and nitrate were generally low, decreased slightly with depth, and oscillated between 2

and 6  $\mu\text{M}$  and between 7 and 12  $\mu\text{M}$ , respectively (Fig. 1A right panel). In turn, the concentration of ammonium generally increased with depth below 18 mm as expected from the decomposition of organic matter during anaerobic Mn(IV) and Fe(III) respiration. Dissolved sulphides or  $\text{FeS}_{(\text{aq})}$  clusters, indicative of sulphate reduction (Beckler *et al.*, 2016), were not detected in these sediments. Overall, these profiles indicate that metal reduction dominates these sediments and suggest that  $\text{Mn}^{3+}$ , Mn + III or +IV and Fe(III)-reducing microbial communities may be separated vertically.

#### *Mn<sup>3+</sup> reduction activity in enrichment cultures and in Shewanella isolates*

To identify microbes mediating acetate oxidation coupled to  $\text{Mn}^{3+}$  reduction, we enriched a microbial community from the  $\text{Mn}^{2+}$ -rich zone between the oxic and Fe(III)-reducing layers of these salt marsh sediments (hatched area in Fig 1A). The enrichment continued to sustain  $\text{Mn}^{3+}$  reduction from soluble  $\text{Mn}^{3+}$  ( $\text{Mn}^{3+}$ -pyrophosphate) with acetate as the sole electron donor under anoxic conditions, after seven transfers spanning two years. At this transfer, 16S rRNA gene amplicon analysis revealed that the culture was dominated by *Shewanella* (Supporting Information Fig. S1). Sulphides were not detected in the cultures that showed  $\text{Mn}^{3+}$  reduction, and the rate of reduction of  $\text{Mn}^{3+}$  did not increase with increasing sulphate concentrations in the medium (Fig 1B), suggesting that  $\text{Mn}^{3+}$  reduction was not mediated by dissolved sulphides. Lack of sulphur resulted in decreased Mn reduction, probably due to lack of S for assimilation, as no sulphides were detected in sulphate-amended cultures and addition of molybdate enhanced  $\text{Mn}^{3+}$  reduction. Finally,  $\text{Mn}^{3+}$  reduction only occurred in the absence of respiratory and growth inhibitors (Fig 1C), confirming the direct and biological nature of  $\text{Mn}^{3+}$  reduction by the microbial community.

From this enrichment, we recovered an isolate, strain MN01 that displayed 98% whole genome average nucleotide identity to *Shewanella algae* BrY (Caccavo *et al.*, 1992) sequenced in this study and 100% to *S. algae* ACDC (Clark *et al.*, 2013)=JCM 21037<sup>T</sup> and 99% to *S. halotis* DW01<sup>T</sup> (Kim *et al.*, 2007) (hereafter the '*S. algae* clade', since 16S rRNA gene (Supporting Information Fig. S2), and whole genome sequence suggest that *S. halotis* DW01<sup>T</sup> is a *S. algae* genomic species (Szeinbaum *et al.* submitted).

Members of the genus *Shewanella* are described as incomplete oxidizers of organic carbon, producing acetate as a result of the anaerobic oxidation of 3C compounds such as lactate (Hunt *et al.*, 2010; Pinchuk *et al.*, 2011; Lovley, 2013). Recently, *S. loihica* PV-4 and *S. denitrificans* were reported to use acetate as electron donor for nitrate reduction, but not metal reduction (Yoon *et al.*, 2013). Strain MN-01, unlike any other *Shewanella* strain studied

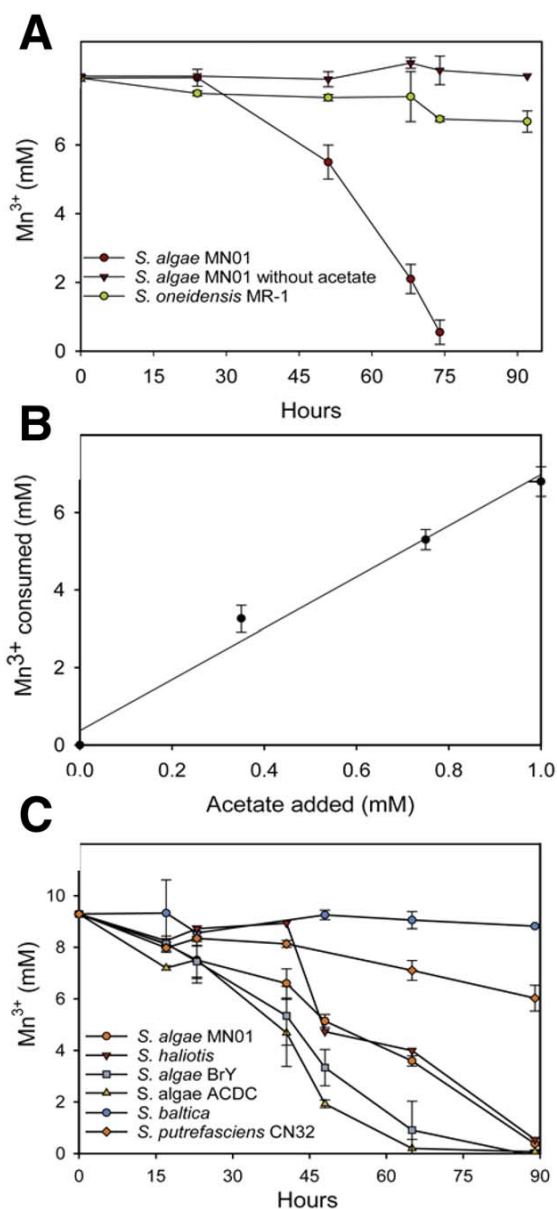


**Fig. 2.** Acetate-dependent  $\text{Mn}^{3+}$  reduction activity in *Shewanella algae* strain MN-01 under anoxic conditions. (A)  $\text{Mn}^{3+}$ -reduction activity during anaerobic incubations with excess or lack of acetate in isolate *S. algae* MN-01. *S. oneidensis* MR-1, unable to reduce  $\text{Mn}^{3+}$  with acetate as electron donor, is added here as a negative control; (B) The extent of acetate-dependent  $\text{Mn}^{3+}$  reduction activity correlates directly with acetate concentrations; (C)  $\text{Mn}^{3+}$  reduction ability with acetate as the sole electron donor by different *Shewanella* strains. [Colour figure can be viewed at [wileyonlinelibrary.com](http://wileyonlinelibrary.com)]

thus far, couples oxidation of acetate to reduction of either soluble  $\text{Mn}^{3+}$  pyrophosphate (Fig. 2A) or  $\text{Fe}^{3+}$ -citrate (Supporting Information Fig. S7A). Like all other metal-

reducing *Shewanella*, strain MN-01 also uses lactate for metal reduction (Supporting Information Fig. S7B). To determine the stoichiometric relationship between the consumption of acetate and  $\text{Mn}^{3+}$ , we carried out incubations with increasingly limiting acetate concentrations and measured the corresponding changes in  $\text{Mn}^{3+}$  reduction (Fig. 2B). The increase in the extent of  $\text{Mn}^{3+}$  consumption as a function of acetate concentration suggests direct coupling of  $\text{Mn}^{3+}$  reduction to respiration. Under our experimental conditions, the relationship between acetate consumed and  $\text{Mn}^{3+}$  reduced is 1:6 (Fig. 2B and Supporting Information Fig. S10) less than the theoretical maximum if acetate is completely oxidized to  $\text{CO}_2$ , in which 8 electrons will reduce 8 molecules of  $\text{Mn}^{3+}$  to  $\text{Mn}^{2+}$ . In anoxic incubations of strain MN-01, dissolved inorganic carbon ( $^{13}\text{C}$ DIC) was produced from  $^{13}\text{C}$ -acetate only in the presence of  $\text{Mn}^{3+}$ , but was absent in  $\text{Mn}^{3+}$ -free, heat-killed, or abiotic controls, confirming that acetate oxidation is biologically mediated and coupled to metal reduction. In these incubations, we observe this 1:8 ratio between  $^{13}\text{C}$ -DIC produced and  $\text{Mn}^{3+}$  reduced. Thus, the fs/fe – or ratio of electrons destined for synthesis (fs) vs. energy generation (fe) (Rittmann and McCarty, 2012) is approximately 1:3, indicating that 75% of the acetate consumed is used for energy generation (a detailed description of our calculations can be found in the supplementary section). The minor proportion (25%) of acetate not used for energy generation may be directed for synthesis. In accordance, under our growth conditions, we measured an increase in 16S rRNA copy numbers in strain MN01 from  $1 \times 10^8$  to  $4 \times 10^8$  right before the onset of Mn reduction (Supporting Information Fig. S10), suggesting that acetate consumption with  $\text{Mn}^{3+}$  reduction is predominantly an energy-generating process.

Equal rates and extent of  $^{13}\text{C}$ DIC production (Fig. 3A) and  $\text{Mn}^{3+}$  consumption (Fig. 3B) by MN-01 with  $^{13}\text{C}$ -C1- and  $^{13}\text{C}$ -C2-labelled acetate demonstrates complete oxidation of acetate to  $\text{CO}_2$ . To ensure that the acetate-oxidizing capacity of MN01 is not an artefact of the enrichment conditions, we also tested *S. algae* strains JCM 21037, BrY and *S. halotis* for  $\text{Mn}^{3+}$  reduction. These strains were isolated under a variety of conditions, on a global scale. Growth on acetate and lactate (Supporting Information Figs. S3–S6) showed that the strains had similar growth rates under 1–2% NaCl, and thus  $\text{Mn}^{3+}$  reduction rates were comparable under these conditions to avoid inherent growth rate differences. All of the *S. algae* strains tested, as well as *S. halotis*, were capable of  $\text{Mn}^{3+}$  reduction with acetate (Fig. 2C), thus expanding the ecological niche of the *Shewanella* genus. Microbial  $\text{Mn}^{3+}$  reduction fuelled by anaerobic acetate oxidation may thus be an underappreciated pathway for organic matter mineralization (Madison et al., 2013; Vedamati et al., 2015).

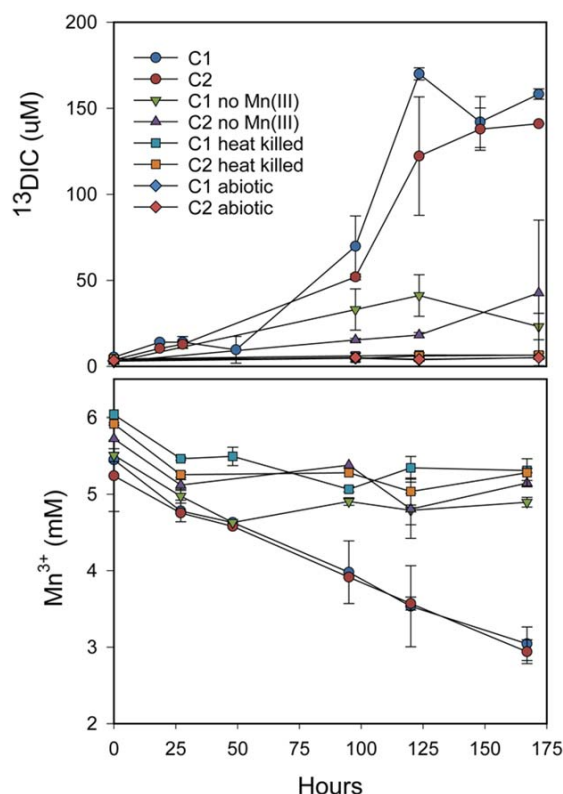


**Fig. 3.** Complete acetate oxidation in isolated strain *Shewanella algae* strain MN-01. A.  $^{13}\text{C}$  labelled dissolved inorganic carbon ( $^{13}\text{C}$ DIC) produced during anaerobic incubations of *S. algae* MN-01 with  $\text{Mn}^{3+}$  as electron acceptor and  $^{13}\text{C}$ -labelled acetate at C1 or C2. B.  $\text{Mn}^{3+}$  reduction rates during incubations with  $^{13}\text{C}$ -labelled acetate. [Colour figure can be viewed at [wileyonlinelibrary.com](http://wileyonlinelibrary.com)]

#### Potential biochemical pathways for acetate oxidation coupled to metal reduction

The metabolic pathway for anaerobic acetate oxidation by metal-reducing bacteria has only been examined in *G. sulfurreducens* and *G. metallireducens* (Galushko and Schink, 2000; Tang et al., 2007). In *Geobacter*, anaerobic acetate oxidation proceeds with the reverse TCA cycle in the oxidative direction. The TCA cycle is typically described as oxidative or reductive, reflecting the roles they played in the organisms where these cycles were discovered, but not their underlying biochemistry. At least three types of TCA cycles work oxidatively but are biochemically distinct. One of the key differences lie in the enzymes that transform 2-oxoglutarate, and are: (i) 2-oxoglutarate dehydrogenase, (ii) 2-oxoglutarate:ferredoxin oxidoreductase and (iii) 2-oxoglutarate carboxylase which leads to a succinyl-coA bypass with succinate semialdehyde dehydrogenase producing succinate. Although these



distinctions are not typically emphasized these differences may reflect underlying evolutionary and ecological forces.

More appropriate is to characterize the reverse (reductive) TCA cycle in *Geobacter* as ferredoxin-driven, the general feature of this cycle, and specify whether it is operating in the oxidative or reductive direction. The ferredoxin-driven TCA cycle is characterized by three key enzymes: (i) 2-oxoglutarate:ferredoxin oxidoreductase (2-OFOR), which oxidizes 2-oxoglutarate to succinyl CoA, (ii) citrate lyase and (iii) pyruvate:ferredoxin oxidoreductase (Thauer, 1988) (Fig. 4A and B left). These highly O<sub>2</sub>-sensitive enzymes, are reversible, enabling the ferredoxin-driven TCA to be used for autotrophy (Thauer, 1988; Hugler *et al.*, 2005). Another unique trait of the ferredoxin-driven TCA pathway in *Geobacter* is the generation of acetyl-CoA by succinylCoA:acetyl-CoA transferase, bypassing phosphorylation of acetate (Thauer, 1988; Galushko and Schink, 2000). The use of ferredoxin, NADP and succinyl-CoA transferase allows the ferredoxin-driven TCA cycle to transfer electrons to acceptors with lower redox potential such as sulphate and metals. Indeed, sulphate-reducing Deltaproteobacteria oxidize acetate anaerobically via the ferredoxin-driven TCA cycle (Thauer, 1988) (Fig. 4B left). Gammaproteobacteria such as *Shewanella*, however, are facultative anaerobes that do not encode the ferredoxin-driven TCA cycle. Instead, oxidoreductases are replaced by non-reversible dehydrogenases, rendering them oxygen-tolerant but limiting this cycle to heterotrophy, (Thauer, 1988) (Fig. 4B right). Thus, we will refer to the heterotrophic, oxygen-tolerant cycle as dehydrogenase-driven, in contrast to ferredoxin-driven. A complete dehydrogenase-driven TCA cycle has not yet been described as a pathway for acetyl-CoA oxidation coupled to energy generation under anoxic conditions, except in Cyanobacteria. In Cyanobacteria, however, 2-oxoglutarate decarboxylase (2OGDC) and succinate semialdehyde dehydrogenase (SSDH) convert 2-oxoglutarate to succinate and generate NADPH (Zhang and Bryant, 2011), bypassing the generation of succinyl-CoA from either 2-OFOR or 2-oxoglutarate dehydrogenase.

To identify possible pathways mediating complete acetate oxidation, we compared the genomes of the *Shewanella* strains with and without the capability of acetate oxidation coupled to Mn<sup>3+</sup> reduction to identify possible pathways mediating complete acetate oxidation. We also compared the central metabolic differences between other facultative and strictly anaerobic metal-reducing proteobacteria. The gammaproteobacterium *Pantoea agglomerans*, the only other facultative anaerobe reported to reduce Fe(III) with acetate (Francis *et al.*, 2000), was included along with Betaproteobacterium *Rhodospirillum rubrum* (Finneran *et al.*, 2003). No Epsilon- and Alphaproteobacterial isolates are available that couple acetate oxidation to metal reduction.

Four distinct enzymes involved in the TCA cycle - aconitate hydratase 2 (AcnA) (Supporting Information Table S1), SSDH (Supporting Information Table S1), and two NADPH:quinone oxidoreductases (Supporting Information Table S1) (Jordan *et al.*, 1999) - may allow metal-reducing Gammaproteobacteria to use acetate (Fig. 4A, highlighted in grey). These enzymes are absent from *Shewanella* species unable to couple acetate oxidation to metal reduction. The genes involved in carbon metabolism and energy generation in the *S. oneidensis* MR-1 and *Shewanella* MN01 genomes are available in the supplementary section (Supporting Information Tables S1–S7, Fig. 4A). *S. algae* encodes two aconitate hydratases, AcnA and AcnB, which isomerize citrate to isocitrate in the TCA cycle. AcnA is more stable, displays a higher affinity for citrate, and operates over a wider pH range than AcnB (Jordan *et al.*, 1999), the only aconitate hydratase encoded by all other *Shewanella* genomes. Among the genomes analysed in this study Cyanobacterial-like SSDH containing the GabD1 domain is only found in Gammaproteobacteria and is absent from non-metal reducing members (Fig. 4B), which only contain the semialdehyde dehydrogenase with a mitochondrial GabH domain. When respiring anaerobically, the NADP<sup>+</sup>/NADPH couple has a redox potential more negative than NAD/NADH (–370 vs. –280 mV), closer to the redox potential of ferredoxin (–400 mV) (Wang *et al.*, 2013). Thus, a NADP-dependent (mena)quinone oxidoreductase may allow the dehydrogenase-driven TCA cycle to reduce electron acceptors other than O<sub>2</sub>. The other described route for acetate oxidation is the oxidative acetyl-CoA pathway (Wood-Ljungdahl pathway) (Hori *et al.*, 2011; Ticak *et al.*, 2014), but the absence of genes encoding the acetyl-CoA synthase/carbon monoxide dehydrogenase complex (Supporting Information Table S2) renders this pathway unlikely in *Shewanella*. Strain MN-01 also encodes the complete *mtr* pathway necessary for Mn<sup>3+</sup> reduction in *Shewanella* (Szeinbaum *et al.*, 2014). Based on our comparative genomic analysis, and considering that both C1 and C2 from acetate are oxidized to CO<sub>2</sub>, we propose that in *S. algae*, acetate oxidation during Mn<sup>3+</sup> reduction proceeds via the complete dehydrogenase-driven TCA cycle, perhaps using the SSDH bypass that Cyanobacteria employ as an obligate route.

#### Environmental implications of acetate oxidation with Mn<sup>3+</sup> reduction supported by distinct TCA cycles

Recent findings indicate that dissimilatory Mn(IV) reduction undergoes two successive one-electron transfer steps and suggest that Mn(IV) is first solubilized by reduction to Mn<sup>3+</sup>, which is then respired as the terminal electron acceptor linked to energy generation (Hui *et al.*, 2012). In accordance, our results show that acetate oxidation can be linked to Mn<sup>3+</sup> reduction at millimolar levels (pure cultures) as well as with environmentally relevant concentrations

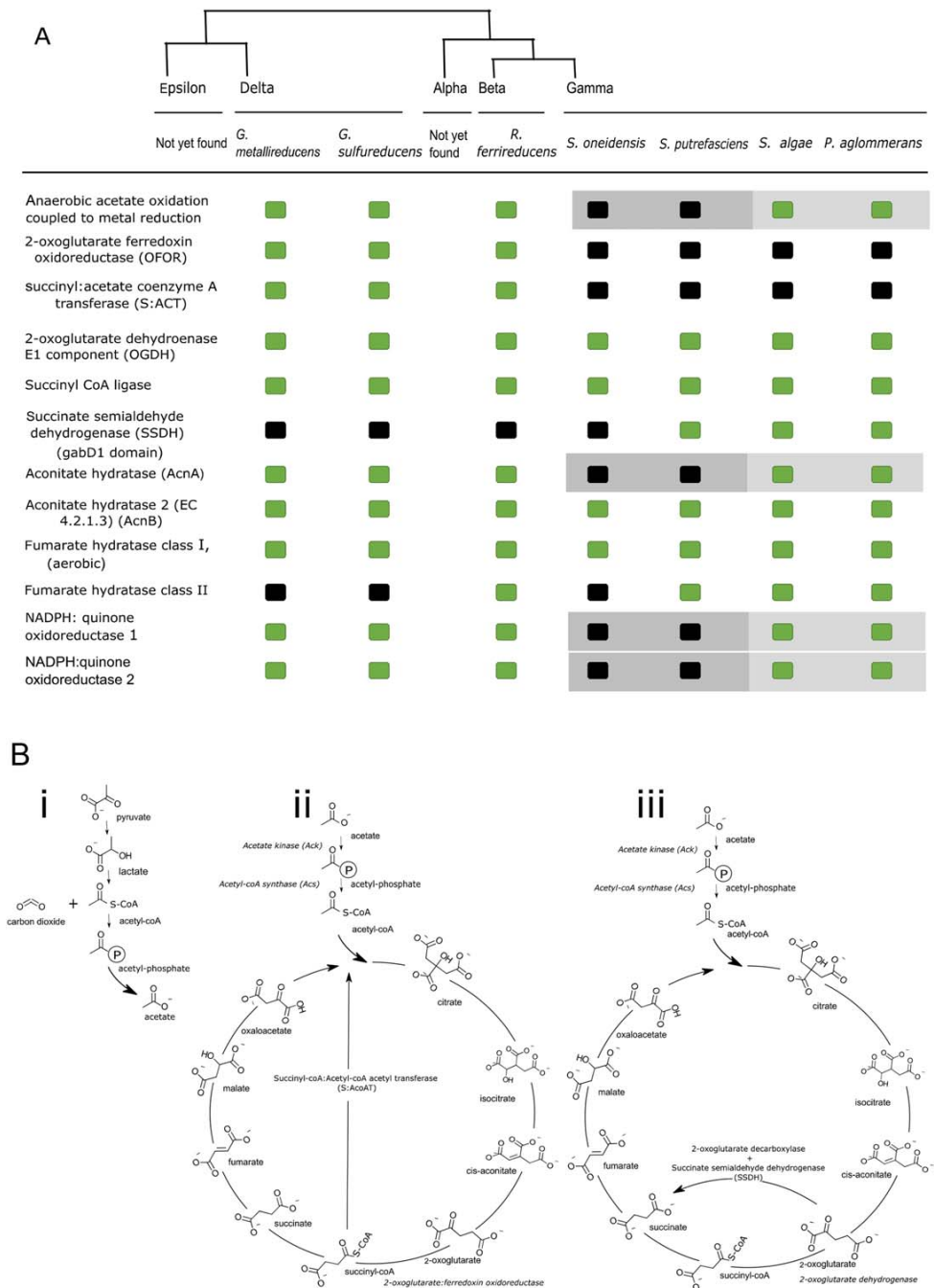


**Fig. 4.** Genetic comparison among metal-reducing Proteobacteria.

**A.** Genes linked to energy generation via the TCA cycle in proteobacteria during acetate-driven metal reduction. Green and black boxes indicate presence and absence of the gene respectively, in each strain. Shaded boxes highlight major differences in the TCA cycle between acetate oxidizers and non-oxidizers. Phylogenetic relationships between proteobacterial lineages are only for reference and not to scale.

**B.** Differences in the biochemistry of carbon oxidation between *Shewanella* and *Geobacter* during (i) incomplete lactate oxidation to acetate by *Shewanella oneidensis* MR-1 and acetate oxidation in (ii) *Geobacter* and (iii) proposed pathway for complete lactate oxidation to CO<sub>2</sub> in *Shewanella algae*. [Colour figure can be viewed at [wileyonlinelibrary.com](http://wileyonlinelibrary.com)]

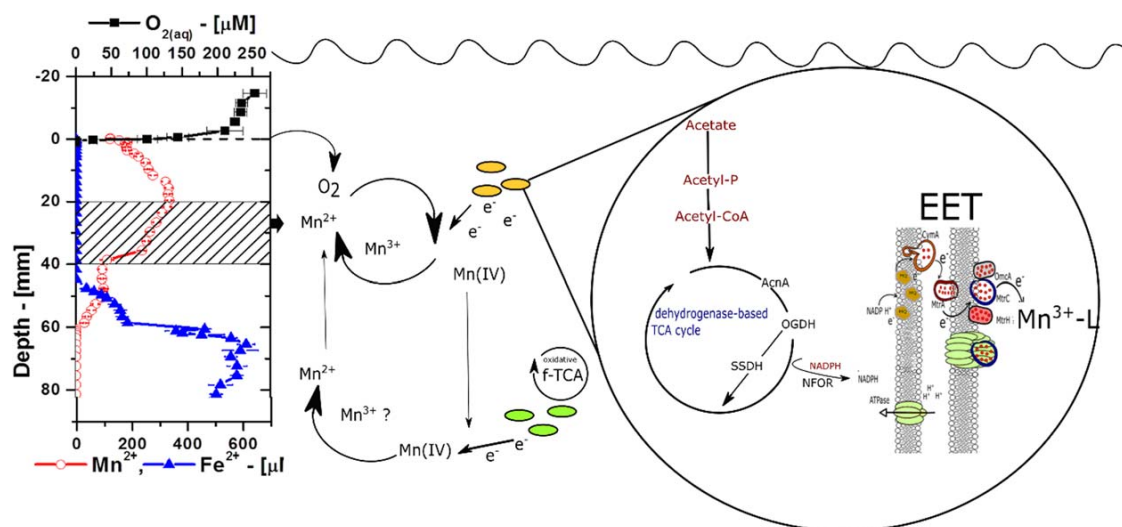


**Fig. 5.** Working model of anaerobic acetate oxidation coupled to  $\text{Mn}^{3+}$  reduction by *Shewanella* in suboxic zones.  $\text{Mn(III)}$  is produced by  $\text{Mn(IV)}$  reduction or  $\text{Mn(II)}$  oxidation below the oxycline, and above ferruginous and sulphidic zones. Gammaproteobacteria such as *Shewanella* can utilize  $\text{Mn}^{3+}$  as an extracellular electron acceptor and persist under redox and carbon and electron acceptor fluctuations. [Colour figure can be viewed at [wileyonlinelibrary.com](http://wileyonlinelibrary.com)]

(enrichment cultures). Widespread detection of soluble  $\text{Mn}^{3+}$  suggest that siderophore- or humic-stabilized  $\text{Mn}^{3+}$  in sediments (Madison *et al.*, 2011; 2013) and water columns (Trouwborst *et al.*, 2006; Dellwig *et al.*, 2012; Schnetger *et al.*, 2012; Oldham *et al.*, 2017) plays an important but overlooked role as an energy-generating electron acceptor to heterotrophs (Hansel, 2017). An oxygen tolerant TCA cycle is a suitable biochemical pathway used by facultative anaerobes for the transfer of electrons from acetate to dissolved  $\text{Mn}^{3+}$  (Fig. 4), under fluctuating redox conditions. The high abundance of  $\text{Mn}^{3+}$  at oxic/anoxic interfaces (Trouwborst *et al.*, 2006; Madison *et al.*, 2013) may be able to support microbial activity and sustain active populations, as other substrates more suitable for growth become available (Fig. 5).

#### Evolutionary implications of acetate oxidation with $\text{Mn}^{3+}$ reduction supported by distinct TCA cycles

Geological evidence for microbial Mn (III/IV) oxides as early as 2.9 Ga and deep phylogenetic origins of metal-reducing microbes support an origin for Mn respiration prior to the Great Oxidation Event at ~2.4 Ga (Crowe *et al.*, 2013; Lovley, 2013; Lyons *et al.*, 2014; Fischer *et al.*, 2015), a period in which oxygenic photosynthesis by Cyanobacteria made oxygen likely available in surface waters. Differences in cytochrome architectures (Bird *et al.*, 2011) between Delta- and Gammaproteobacteria and differences in central metabolism biochemistry suggests that the enzymatic machinery for acetate oxidation coupled to metal reduction might have evolved independently, perhaps

reflecting different oxygen regimes. In this model, strictly anaerobic Deltaproteobacteria (e.g., *Geobacter*) retained the oxygen-sensitive enzymes of the ferredoxin-driven TCA cycle, present today in other Epsilon- and Deltaproteobacteria typically found in sulphidic environments (Johnston *et al.*, 2009; Berg, 2011), Gammaproteobacteria (e.g., *Shewanella*) may have evolved under higher oxygen exposure from photosynthetic activity (Johnston *et al.*, 2009; Lyons *et al.*, 2014; Planavsky *et al.*, 2014; Kurzweil *et al.*, 2016) thus requiring the dehydrogenase-driven TCA cycle, with the potential for an SSDH bypass. This new link between the carbon and manganese cycles in which acetate oxidation fuels soluble  $\text{Mn}^{3+}$  reduction is therefore important to the interpretation of the roles of modern and ancient Mn redox, and Mn-driven carbon cycles.

#### Experimental procedures

##### Sediment sampling and field measurements

Triplicate sediment cores ( $7.5 \times 50$  cm) were collected from a perennial creek bank at the Salt Marsh Ecosystem Research Facility (SERF) of the Skidaway Institute of Oceanography, Georgia as described by (Taillefert *et al.*, 2007). Vertical pore water profiles of the major redox chemical species  $\text{O}_2$ ,  $\text{Mn}^{2+}$ ,  $\text{Fe}^{2+}$ , and  $\sum \text{H}_2\text{S} = (\text{H}_2\text{S} + \text{HS}^- + \text{S}^{(0)} + \text{S}_x^{2-})$  as well as qualitative signals for soluble organic- $\text{Fe}^{3+}$  complexes and  $\text{FeS}_{(\text{aq})}$  molecular clusters were obtained with gold/mercury amalgam (Au/Hg) voltammetric microelectrodes (Luther *et al.*, 2008) linked to a potentiostat (AIS, Model DLK-60) deployed on a computer-controlled micromanipulator (AIS, MAN-1). Dissolved oxygen was quantified by linear sweep voltammetry, while other species were detected by cathodic square wave

voltammetry (Taillefert *et al.*, 2000). All voltammetric measurements were conducted at a scan rate of  $200 \text{ mV s}^{-1}$  from  $-0.1$  to  $-1.8 \text{ V}$  and included a conditioning step of  $10 \text{ s}$  at  $-0.1 \text{ V}$ . When needed, a cleaning step of  $10 \text{ s}$  at  $-0.9 \text{ V}$  was added before each measurement. Voltammograms were integrated using the semi-automatic integration program VOLTINT in Matlab (Bristow and Taillefert, 2008). Pore water was extracted from  $\sim 5 \text{ mm}$  sections of the sediment core by centrifugation (3500 rpm) under  $\text{N}_2$ -atmosphere and analysed for  $\text{NO}_3^-$  and  $\text{NO}_2^-$  by HPLC with UV detection (Beckler *et al.*, 2014) and for  $\text{NH}_4^+$  spectrophotometrically (Riley, 1953).

#### *Enrichment of microbial communities that couple anaerobic acetate oxidation to $\text{Mn}^{3+}$ reduction*

Enrichment cultures were initiated by transferring  $2.5 \text{ g}$  of homogenized sediment from the  $\text{Mn}^{2+}$ -rich redox zone (30–50 mm depth interval) to  $100 \text{ mL}$  of anaerobic growth medium in serum bottles under a  $\text{N}_2$  atmosphere. Growth medium consisted of sterile sulphate-free artificial seawater (Schut *et al.*, 1993) diluted two-fold with anoxic deionized water to mimic salt marsh ionic strength. Replicate enrichments were amended with either  $100 \mu\text{M}$ ,  $1 \text{ mM}$ , or  $14 \text{ mM}$  sodium sulphate. Soluble  $\text{Mn}^{3+}$  (as  $\text{Mn}^{3+}$ -pyrophosphate) and acetate were both added to final concentrations of  $200 \mu\text{M}$  from anoxic stock solutions using an  $\text{N}_2$ -flushed syringe.  $\text{Mn}^{3+}$ -pyrophosphate stock solutions were prepared by solubilization of  $500 \text{ mM}$   $\text{Mn}_2\text{O}_3$  in  $40 \text{ mM}$  sodium pyrophosphate at  $\text{pH } 6.5$  (Kostka *et al.*, 1995). The enrichments were incubated at room temperature in the dark and  $5\%$  (v/v) aliquots were transferred to fresh media every 45–60 days with an  $\text{N}_2$ -flushed syringe.

#### *Inhibition of microbial $\text{Mn}^{3+}$ reduction activity*

A set of control enrichment cultures was incubated in the presence of a suite of metabolic inhibitors to differentiate between microbial and chemical  $\text{Mn}^{3+}$  reduction activity. The bacterial sulphate reduction inhibitor sodium molybdate ( $14$  and  $140 \text{ mM}$ ) was added to determine if sulphide produced by sulphate-reducing bacteria acted as an electron shuttle to  $\text{Mn}^{3+}$  (i.e., the enrichment conditions selected for sulphate- and not  $\text{Mn}^{3+}$ -reducing bacteria). The antibiotics ampicillin ( $1.1$  and  $2.3 \text{ mM}$ ) and chloramphenicol ( $62$  and  $620 \mu\text{M}$ ) were also added to replicate enrichment cultures to confirm the microbial basis of  $\text{Mn}^{3+}$  reduction activity. Respiratory inhibitors 2,4 dinitrophenol ( $360$  and  $3600 \mu\text{M}$ ) and carbonyl cyanide *m*-chlorophenylhydrazone (CCCP,  $200 \mu\text{M}$ ), were added to assess whether  $\text{Mn}^{3+}$  reduction activity was electron transport chain-linked.

#### *Cultivation-independent phylogenetic affiliation of the dominant populations of the enrichment*

Biomass from the enrichment cultures displaying  $\text{Mn}^{3+}$  reduction activity with acetate as electron donor was collected by centrifugation ( $10\,000 \times g$ ,  $25 \text{ min}$  at  $\text{RT}$ ). Total community DNA was extracted and purified by standard phenol:chloroform extraction (Sambrook and Russell, 2006). The 16S SSU rRNA gene was amplified using universal primers U1

corresponding to the V1-3 hypervariable region (Supporting Information Table S1). Approximately  $30 \text{ ng}$  of enriched community DNA was used in  $50 \mu\text{L}$  PCR reaction mixtures consisting of iProof DNA polymerase (BioRad) and an annealing temperature of  $40^\circ\text{C}$ . The amplification product was purified by electrophoretic separation on  $1.5\%$  agarose gels (Qiagen) prior to library construction. Emulsion PCR was carried out according to the manufacturer's instructions. Sequencing of the 16S rDNA amplicon libraries was carried out on a 314 chip using the Ion Torrent PGM system. Taxonomic assignment of amplified nucleotide sequence analyses were carried out with Galaxy, an open source, web-based platform for genomic analyses (Blankenberg *et al.*, 2010).

#### *Isolation and phylogenetic assignment of purified bacterial strains that couple anaerobic acetate oxidation to $\text{Mn}^{3+}$ reduction*

Aliquots from the enrichment cultures displaying  $\text{Mn}^{3+}$  reduction activity were serially-diluted and spread on agar growth medium and incubated for 5–7 days under anoxic conditions. For phylogenetic identification of the purified strains, total DNA was extracted from single purified bacterial colonies, and subsequently used as template for PCR amplification of full-length 16S rDNA with primers 8F and 1489R. The resulting sequence was queried against the nucleotide collection using nBLAST search (NCBI).

Genomic DNA from isolated strain *Shewanella* strain MN01 and *S. algae* strain BrY (ATCC 51181) was purified with a DNA purification kit (Sigma-Aldrich, St. Louis, MO) after growth of an overnight culture in LB at  $37^\circ\text{C}$  and sequenced at the Center for Integrative Genomics (Georgia Institute of Technology, Atlanta, GA). DNA was sheared by sonication (Sonicman, Brooks Automation, Spokane, WA) to an average insert size of  $650 \text{ bp}$ , and DNA libraries were prepared for Illumina paired-end sequencing as described by the manufacturer (Illumina, San Diego, CA). Libraries were sequenced to a read length of  $100 \text{ bp}$  on an Illumina HiSeq 2500 system. Genome assembly of the resulting  $11\,649\,110$  paired-end reads was carried out in CLC Genomics Workbench 8.0.2 (CLC Bio-Qiagen, Aarhus, Denmark; <http://www.clbio.com>). Reads were filtered based on quality scores (discarding sequences with at least one N) and length ( $> 90 \text{ nt}$ ). Contigs  $< 2000 \text{ bp}$  were removed from further analysis. De novo assembly generated a total of  $129$  contigs with an average length of  $47\,187 \text{ bp}$  and average coverage of  $140$ . The resulting genome sequences have been deposited at DDBJ/EMBL/GenBank under the accession numbers LIRM000000000 (*S. algae* MN01) and MDA000000000 (*S. algae* BrY).

#### *Analytical methods*

$\text{Mn}^{2+}$  and  $\sum \text{H}_2\text{S}$  concentrations in the enrichment and pure cultures were determined by cathodic square wave voltammetry as described above.  $\text{Mn}^{3+}$  reduction was monitored spectrophotometrically by absorbance at  $480 \text{ nm}$  of culture supernatants filtered through  $0.2 \mu\text{m}$  pore filters (Kostka *et al.*, 1995). Fe(III) reduction activity was monitored by following the production of  $\text{Fe}^{2+}$  via the ferrozine method (Stookey, 1970).



Quantification of acetate was performed with an Agilent 1100 series HPLC and a UV-VIS detector at 210 nm. Acetate was quantified by HPLC (Agilent 1100 series) with UV detection at 210 nm using a Supelcogel™ C-610H ion exclusion column (30 × 7.8 mm) employing an isocratic method with 0.1% phosphoric acid as the eluent at a flow rate of 0.3 ml/min. Samples for total dissolved inorganic carbon isotope ( $\delta^{13}\text{C}$ -DIC) analysis were collected into 2 ml crimp-seal autosampler vials fitted with 500  $\mu\text{l}$  glass inserts. Samples were analysed for  $\delta^{13}\text{C}$ -DIC and [DIC] using a liquid chromatography-isotope ratio mass spectrometry (LC-IRMS) using an Isolink interface coupled to a ThermoFisher Delta V+ IRMS (Brandes, 2009). Although measured precision is lower in vials with inserts compared to without, the reduced sample volume allowed us to sample incubations more frequently. The system was calibrated with sodium bicarbonate standards in Milli-Q water (0–2500  $\mu\text{M}$  DIC). Isotope and concentration standardization was accomplished using  $\text{NaHCO}_3$  solutions, made by directly weighing the solid into 25 ml volumetric flasks, adding deionized water, sealing with Parafilm and rapidly mixing. Solutions were then rapidly transferred to 2 ml crimp-seal vials and sealed with Teflon-faced butyl-rubber septa (Brandes, 2009). The laboratory internal standard  $\text{NaHCO}_3$  was calibrated against the NBS 19 calcite standard using a ThermoFisher Gasbench II interfaced to the Delta V+ IRMS (Torres *et al.*, 2005), and all isotope values are reported versus the VPDB (Vienna Pee Dee Belemnite) reference scale (Allison *et al.*, 1995).

## Acknowledgements

This work was supported by NSF Geobiology and Low Temperature Geochemistry grant 0922243 awarded to M.T. and T.J.D., NSF Chemical Oceanography grant 1234704 awarded to J.A.B. and a NASA Exobiology Grant NNX14AJ87G awarded to J.B.G. and T.J.D.

## References

- Allison, C.E., Francey, R.J., and Meijer, H.A.J. (1995) Recommendations for the reporting of stable isotope measurements of carbon and oxygen in  $\text{CO}_2$  gas, in Reference and Intercomparison Materials for Stable Isotopes of Light Elements, IAEA-Tech. Doc.-825. Vienna, Austria: International Atomic Energy Agency, pp. 155–162.
- Balba, M.T., and Nedwell, D.B. (1982) Microbial-metabolism of acetate, propionate and butyrate in anoxic sediment from the Colne Point Saltmarsh, Essex, UK. *J Gen Microbiol* **128**: 1415–1422.
- Beckler, J.S., Nuzzio, D.B., and Tallefert, M. (2014) Development of single-step liquid chromatography methods with ultraviolet detection for the measurement of inorganic anions in marine waters. *Limnol Oceanogr-Methods* **12**: 563–576.
- Beckler, J.S., Jones, M.E., and Tallefert, M. (2015) The origin, composition, and reactivity of dissolved iron(III) complexes in coastal organic- and iron-rich sediments. *Geochim Cosmochim Acta* **152**: 72–88.
- Beckler, J.S., Kiriazis, N., Rabouille, C., Stewart, F.J., and Tallefert, M. (2016) Importance of microbial iron reduction in deep sediments of river-dominated continental-margins. *Mar Chem* **178**: 22–34.
- Berg, I.A. (2011) Ecological aspects of the distribution of different autotrophic  $\text{CO}_2$  fixation pathways. *Appl Environ Microbiol* **77**: 1925–1936.
- Bird, L.J., Bonnefoy, V., and Newman, D.K. (2011) Bioenergetic challenges of microbial iron metabolisms. *Trends Microbiol* **19**: 330–340.
- Blair, N.E., Carter, W.D., and Boehme, S.E. (1991) Diagenetic isotope effects in an anoxic marine sediment. *Abstr Pap Am Chem Soc* **201**: 34.
- Blankenberg, D., Von Kuster, G., Coraor, N., Ananda, G., Lazarus, R., Mangan, M., *et al.* (2010) Galaxy: a web-based genome analysis tool for experimentalists. *Curr Protoc Mol Biol* Chapter 19: Unit 19.10.1–21.
- Brandes, J.A. (2009) Rapid and precise  $\delta^{13}\text{C}$  measurement of dissolved inorganic carbon in natural waters using liquid chromatography coupled to an isotope-ratio mass spectrometer. *Limnol Oceanogr: Methods* **7**: 730–739.
- Bristow, G., and Tallefert, M. (2008) A Matlab-based program for semi-automated processing of geochemical data acquired by voltammetry. *Comput Geosci* **34**: 153–162.
- Caccavo, F., Blakemore, R.P., and Lovley, D.R. (1992) A hydrogen-oxidizing, Fe(III)-reducing microorganism from the great bay estuary, New Hampshire. *Appl Environ Microbiol* **58**: 3211–3216.
- Clark, I.C., Melnyk, R.A., Engelbrektson, A., and Coates, J.D. (2013) Structure and evolution of chlorate reduction composite transposons. *MBio* **4**: e00379–13. Available at <http://doi.org/10.1128/mBio.00379-13>
- Crowe, S.A., Dossing, L.N., Beukes, N.J., Bau, M., Kruger, S.J., Frei, R., *et al.* (2013) Atmospheric oxygenation three billion years ago. *Nature* **501**: 535–538.
- de Graaf, W., Wellsbury, P., Parkes, R.J., and Cappenberg, T.E. (1996) Comparison of acetate turnover in methanogenic and sulfate-reducing sediments by radiolabeling and stable isotope labeling and by use of specific inhibitors: evidence for isotopic exchange. *Appl Environ Microbiol* **62**: 772–777.
- Dellwig, O., Schnetger, B., Brumsack, H.J., Grossart, H.P., and Umlauf, L. (2012) Dissolved reactive manganese at pelagic redoxclines (part II): Hydrodynamic conditions for accumulation. *J Mar Syst* **90**: 31–41.
- Duckworth, O.W., and Sposito, G. (2005) Siderophore-manganese(III) Interactions. II. Manganite dissolution promoted by desferrioxamine B. *Environ Sci Technol* **39**: 6045–6051.
- Duckworth, O.W., and Sposito, G. (2007) Siderophore-promoted dissolution of synthetic and biogenic layer-type Mn oxides. *Chem Geol* **242**: 497–508.
- Elifantz, H., N'guessan, L.A., Mouser, P.J., Williams, K.H., Wilkins, M.J., Rizzo, C., *et al.* (2010) Expression of acetate permease-like (apl) genes in subsurface communities of *Geobacter* species under fluctuating acetate concentrations. *FEMS Microbiol Ecol* **73**: 441–449.
- Ferry, J.G. (2015) Acetate metabolism in anaerobes from the domain archaea. *Life (Basel)* **5**: 1454–1471.
- Finke, N., Vandieken, V., and Jorgensen, B.B. (2007) Acetate, lactate, propionate, and isobutyrate as electron donors for iron and sulfate reduction in Arctic marine sediments, Svalbard. *FEMS Microbiol Ecol* **59**: 10–22.

- Finneran, K.T., Johnsen, C.V., and Lovley, D.R. (2003) *Rhodoferrax ferrireducens* sp. nov., a psychrotolerant, facultatively anaerobic bacterium that oxidizes acetate with the reduction of Fe(III). *Int J Syst Evol Microbiol* **53**: 669–673.
- Fischer, W.W., Hemp, J., and Johnson, J.E. (2015) Manganese and the evolution of photosynthesis. *Orig Life Evol Biosph* **45**: 351–357.
- Francis, C.A., Obraztsova, A.Y., and Tebo, B.M. (2000) Dissimilatory metal reduction by the facultative anaerobe *Pantoea agglomerans* SP1. *Appl Environ Microbiol* **66**: 543–548.
- Froelich, P.N., Klinkhammer, G.P., Bender, M.L., Luedtke, N.A., Heath, G.R., Cullen, D., et al. (1979) Early oxidation of organic-matter in pelagic sediments of the eastern equatorial Atlantic - suboxic diagenesis. *Geochim Cosmochim Acta* **43**: 1075–1090.
- Galushko, A.S., and Schink, B. (2000) Oxidation of acetate through reactions of the citric acid cycle by *Geobacter sulfurreducens* in pure culture and in syntrophic coculture. *Arch Microbiol* **174**: 314–321.
- Hansel, C. (2017) Small but mighty: How minor components drive major biogeochemical cycles. *Environ Microbiol Reports* **9**: 8–10. doi: 10.1111/1758-2229.12481
- Heuer, V.B., Pohlman, J.W., Torres, M.E., Elvert, M., and Hinrichs, K.U. (2009) The stable carbon isotope biogeochemistry of acetate and other dissolved carbon species in deep seafloor sediments at the northern Cascadia Margin. *Geochim Cosmochim Acta* **73**: 3323–3336.
- Hori, T., Sasaki, D., Haruta, S., Shigematsu, T., Ueno, Y., Ishii, M., et al. (2011) Detection of active, potentially acetate-oxidizing syntrophs in an anaerobic digester by flux measurement and formyltetrahydrofolate synthetase (FTHFS) expression profiling. *Microbiology* **157**: 1980–1989.
- Hugler, M., Wirsén, C.O., Fuchs, G., Taylor, C.D., and Sievert, S.M. (2005) Evidence for autotrophic CO<sub>2</sub> fixation via the reductive tricarboxylic acid cycle by members of the epsilon subdivision of proteobacteria. *J Bacteriol* **187**: 3020–3027.
- Hui, L., Szeinbaum, N., DiChristina, T., and Taillefert, M. (2012) Microbial Mn(IV) reduction requires an initial one-electron reductive solubilization step. *Geochim Cosmochim Acta* **99**: 179–192.
- Hui, L., and Taillefert, M. (2014) Key geochemical factors regulating Mn(IV)-catalyzed anaerobic nitrification in coastal marine sediments. *Geochim Cosmochim Acta* **133**: 17–33.
- Hunt, K.A., Flynn, J.M., Naranjo, B., Shikhare, I.D., and Gralnick, J.A. (2010) Substrate-level phosphorylation is the primary source of energy conservation during anaerobic respiration of *Shewanella oneidensis* strain MR-1. *J Bacteriol* **192**: 3345–3351.
- Johnston, D.T., Wolfe-Simon, F., Pearson, A., and Knoll, A.H. (2009) Anoxygenic photosynthesis modulated Proterozoic oxygen and sustained Earth's middle age. *Proc Natl Acad Sci USA* **106**: 16925–16929.
- Jordan, P.A., Tang, Y., Bradbury, A.J., Thomson, A.J., and Guest, J.R. (1999) Biochemical and spectroscopic characterization of *Escherichia coli* aconitases (AcoA and AcoB). *Biochem J* **344** (Part 3): 739–746.
- Kim, D., Baik, K.S., Kim, M.S., Jung, B.M., Shin, T.S., Chung, G.H., et al. (2007) *Shewanella haliotis* sp. nov., isolated from the gut microflora of abalone, *Haliotis discus hannai*. *Int J Syst Evol Microbiol* **57**: 2926–2931.
- Kostka, J.E., Luther, G.W., and Nealson, K.H. (1995) Chemical and biological reduction of Mn(III)-pyrophosphate complexes - potential importance of dissolved Mn(III) as an environmental oxidant. *Geochim Cosmochim Acta* **59**: 885–894.
- Kurzweil, F., Wille, M., Gantert, N., Beukes, N.J., and Schoenberg, R. (2016) Manganese oxide shuttling in pre-GOE oceans – evidence from molybdenum and iron isotopes. *Earth Planetary Sci Lett* **452**: 69–78.
- Lovley, D. (2013). *Dissimilatory Fe(III)- and Mn(IV)-Reducing Prokaryotes*. The Prokaryotes. Rosenberg, E. (eds). Berlin Heidelberg: Springer-Verlag, pp. 287–305.
- Lovley, D.R. (2008) The microbe electric: conversion of organic matter to electricity. *Curr Opin Biotechnol* **19**: 564–571.
- Lovley, D.R., Holmes, D.E., and Nevin, K.P. (2004) Dissimilatory Fe(III) and Mn(IV) reduction. *Adv Microbial Physiol* **49**: 219–286.
- Luther, G.W., Glazer, B.T., Ma, S.F., Trouwborst, R.E., Moore, T.S., Metzger, E., et al. (2008) Use of voltammetric solid-state (micro)electrodes for studying biogeochemical processes: laboratory measurements to real time measurements with an in situ electrochemical analyzer (ISEA). *Mar Chem* **108**: 221–235.
- Luther, G.W., III, Madison, A.S., Mucci, A., Sundby, B., and Oldham, V. (2015) A kinetic approach to assess the strengths of ligands bound to soluble Mn(III). *Mar Chem* **173**: 93–99.
- Lyons, T.W., Reinhard, C.T., and Planavsky, N.J. (2014) The rise of oxygen in Earth's early ocean and atmosphere. *Nature* **506**: 307–315.
- Madison, A.S., Tebo, B.M., and Luther, G.W. (2011) Simultaneous determination of soluble manganese(III), manganese(II) and total manganese in natural (pore)waters. *Talanta* **84**: 374–381.
- Madison, A.S., Tebo, B.M., Mucci, A., Sundby, B., and Luther, G.W. (2013) Abundant porewater Mn(III) is a major component of the sedimentary redox system. *Science* **341**: 875–878.
- Oldham, V., Owings, C.G., Jones, M., Tebo, R.B., and Luther, G.W., III. (2015) Evidence for the presence of strong Mn(III)-binding ligands in the water column of the Chesapeake Bay. *Mar Chem* **171**: 58–66.
- Oldham, V.E., Mucci, A., Tebo, B.M., and Luther, G.W. (2017) Soluble Mn(III)-L complexes are abundant in oxygenated waters and stabilized by humic ligands. *Geochim Cosmochim Acta* **199**: 238–246.
- Pinchuk, G.E., Geydebrekht, O.V., Hill, E.A., Reed, J.L., Konopka, A.E., Beliaev, A.S., et al. (2011) Pyruvate and lactate metabolism by *Shewanella oneidensis* MR-1 under fermentation, oxygen limitation, and fumarate respiration conditions. *Appl Environ Microbiol* **77**: 8234–8240.
- Planavsky, N., D., Asael, A., Hofmann, C., Reinhard, S., Lalonde, K.A., et al. (2014) Evidence for oxygenic photosynthesis half a billion years before the Great Oxidation Event. *Nat Geosci* **7**: 283–286.
- Post, J.E. (1999) Manganese oxide minerals: crystal structures and economic and environmental significance. *Proc Natl Acad Sci USA* **96**: 3447–3454.
- Ragsdale, S.W., and Pierce, E. (2008) Acetogenesis and the Wood-Ljungdahl pathway of CO<sub>2</sub> fixation. *Biochim Biophys Acta* **1784**: 1873–1898.

- Riley, J.P. (1953) The spectrophotometric determination of ammonia in natural waters with particular reference to sea-water. *Anal Chim Acta* **9**: 575–589.
- Rittmann, B.E., and McCarty, P.L. (2012) *Environmental Biotechnology: Principles and Applications*. Boston, MA: Tata McGraw-Hill Education.
- Russell, M.J., and Martin, W. (2004) The rocky roots of the acetyl-CoA pathway. *Trends Biochem Sci* **29**: 358–363.
- Sambrook, J., and Russell, D.W. (2006) Purification of nucleic acids by extraction with phenol:chloroform. *CSH Protoc* **2006**. doi: 10.1101/pdb.prot4455
- Schnetger, B., and Dellwig, O. (2012) Dissolved reactive manganese at pelagic redoxclines (part I): A method for determination based on field experiments. *J Mar Syst* **90**: 23–30.
- Schut, F., de Vries, E.J., Gottschal, J.C., Robertson, B.R., Harder, W., Prins, R.A., et al. (1993) Isolation of typical marine bacteria by dilution culture: growth, maintenance, and characteristics of isolates under laboratory conditions. *Appl Environ Microbiol* **59**: 2150–2160.
- Stookey, L.L. (1970) Ferrozine. A new spectrophotometric reagent for iron. *Anal Chem* **42**: 779.
- Szeinbaum, N., Burns, J.L., and DiChristina, T.J. (2014) Electron transport and protein secretion pathways involved in Mn(III) reduction by *Shewanella oneidensis*. *Environ Microbiol Rep* **6**: 490–500.
- Taillefert, M., Bono, A.B., and Luther, G.W. (2000) Reactivity of freshly formed Fe(III) in synthetic solutions and (pore)-waters: Voltammetric evidence of an aging process. *Environ Sci Technol* **34**: 2169–2177.
- Taillefert, M., Neuhuber, S., and Bristow, G. (2007) The effect of tidal forcing on biogeochemical processes in intertidal salt marsh sediments. *Geochem Trans* **8**: 1–15.
- Tang, Y.J., Chakraborty, R., Martin, H.G., Chu, J., Hazen, T.C., and Keasling, J.D. (2007) Flux analysis of central metabolic pathways in *Geobacter metallireducens* during reduction of soluble Fe(III)-nitrilotriacetic acid. *Appl Environ Microbiol* **73**: 3859–3864.
- Tebo, B.M., Johnson, H.A., McCarthy, J.K., and Templeton, A.S. (2005) Geomicrobiology of manganese(II) oxidation. *Trends Microbiol* **13**: 421–428.
- Thauer, R.K. (1988) Citric-acid cycle, 50 years on. Modifications and an alternative pathway in anaerobic bacteria. *Eur J Biochem* **176**: 497–508.
- Ticak, T., Kountz, D.J., Girosky, K.E., Krzycki, J.A., and Ferguson, D.J. Jr. (2014) A nonpyrrolysine member of the widely distributed trimethylamine methyltransferase family is a glycine betaine methyltransferase. *Proc Natl Acad Sci USA* **111**: E4668–E4676.
- Tor, J.M., Kashefi, K., and Lovley, D.R. (2001) Acetate oxidation coupled to Fe(III) reduction in hyperthermophilic microorganisms. *Appl Environ Microbiol* **67**: 1363–1365.
- Torres, M.E., Mix, A.C., and Rugh, W.D. (2005) Precise  $\delta^{13}\text{C}$  analysis of dissolved inorganic carbon in natural waters using automated headspace sampling and continuous-flow mass spectrometry. *Limnol Oceanogr: Methods* **3**: 349–360.
- Trouwborst, R.E., Clement, B.G., Tebo, B.M., Glazer, B.T., and Luther, G.W. (2006) Soluble Mn(III) in suboxic zones. *Science* **313**: 1955–1957.
- Vandieken, V., Pester, M., Finke, N., Hyun, J.H., Friedrich, M.W., Loy, A., et al. (2012) Three manganese oxide-rich marine sediments harbor similar communities of acetate-oxidizing manganese-reducing bacteria. *ISME J* **6**: 2078–2090.
- Vandieken, V., and Thamdrup, B. (2013) Identification of acetate-oxidizing bacteria in a coastal marine surface sediment by RNA-stable isotope probing in anoxic slurries and intact cores. *FEMS Microbiol Ecol* **84**: 373–386.
- Vandieken, V., Finke, N., and Thamdrup, B. (2014) Hydrogen, acetate, and lactate as electron donors for microbial manganese reduction in a manganese-rich coastal marine sediment. *FEMS Microbiol Ecol* **87**: 733–745.
- Vedamati, J., Chan, C., and Moffett, J.W. (2015) Distribution of dissolved manganese in the Peruvian Upwelling and Oxygen Minimum Zone. *Geochim Cosmochim Acta* **156**: 222–240.
- Wang, S., Huang, H., Kahnt, J., Mueller, A.P., Kopke, M., and Thauer, R.K. (2013) NADP-specific electron-bifurcating [FeFe]-hydrogenase in a functional complex with formate dehydrogenase in *Clostridium autoethanogenum* grown on CO. *J Bacteriol* **195**: 4373–4386.
- Webb, S.M., Dick, G.J., Bargar, J.R., and Tebo, B.M. (2005) Evidence for the presence of Mn(III) intermediates in the bacterial oxidation of Mn(II). *Proc Natl Acad Sci USA* **102**: 5558–5563.
- Yakushev, E., Pakhomova, S., Sorenson, K., and Skei, J. (2009) Importance of the different manganese species in the formation of water column redox zones: Observations and modeling. *Mar Chem* **117**: 59–70.
- Yoon, S., Sanford, R.A., and Löffler, F.E. (2013) *Shewanella* spp. use acetate as an electron donor for denitrification but not ferric iron or fumarate reduction. *Appl Environ Microbiol* **79**: 2818–2822.
- Zhang, S., and Bryant, D.A. (2011) The tricarboxylic acid cycle in cyanobacteria. *Science* **334**: 1551–1553.

### Supporting information

Additional Supporting Information may be found in the online version of this article at the publisher's web-site:

**Fig. S1.** Mn(III) reduction activity of the 2-year enriched culture. (A) Abundance distribution of major taxa detected via Ion Torrent 16S SSU rRNA amplicon sequencing.

**Fig. S2.** Phylogenetic relationships between isolate MN-01 and other *Shewanella* type strains based on full-length 16S rRNA gene sequences. The tree was constructed using the maximum parsimony method; the bootstrap values (100 replicates) and scale bar of 1 substitution per 100 nt are shown.

**Fig. S3.** Growth of strains (A) *S. haliotis*, (B) *S. algae* BrY, (C) *S. algae* ACDC and (D) strain MN01 with lactate at 37°C under varying NaCl concentrations (%).

**Fig. S4.** Growth of strains (A) *S. haliotis* (B) *S. algae* BrY (C) *S. algae* ACDC and (D) strain MN01 with acetate at 37°C under varying NaCl concentrations (%).

**Fig. S5.** Growth of strains (A) *S. haliotis* (B) *S. algae* BrY (C) *S. algae* ACDC and (D) strain MN01 with lactate at 30°C under varying NaCl concentrations (%).

**Fig. S6.** Growth of strains (A) *S. haliotis*, (B) *S. algae* BrY, (C) *S. algae* ACDC and (D) strain MN01 with acetate at 30°C under varying NaCl concentrations (%).

**Fig. S7.** Growth of strains (A) *S. haliotis*, (B) *S. algae* BrY, (C) *S. algae* ACDC and (D) strain MN01 with lactate at 25°C under varying NaCl concentrations (%).

**Fig. S8.** Growth of strains (A) *S. haliotis*, (B) *S. algae* BrY, (C) *S. algae* ACDC and (D) strain MN01 with acetate at 25°C under varying NaCl concentrations (%).

**Fig. S9.** Mn(III)-reduction activity of the isolated strain *Shewanella algae* MN-01. (A) with lactate or acetate as electron donor and  $\text{Fe}^{3+}$  as electron acceptor; and (B) with lactate or acetate as electron donor and  $\text{Mn}^{3+}$  as electron acceptor.

**Fig. S10.** Incubation of strain MN01 under anaerobic conditions with acetate and  $\text{Mn}^{3+}$ -pyrophosphate. The plot shows acetate consumption (white and,  $\text{Mn}^{3+}$  reduction (light grey)

on the primary axis and 16S rRNA gene copy numbers (dark grey) on the secondary axis.

**Table S1.** Primers used in this study.

**Table S2.** *Shewanella algae* MN-01 genes putatively involved in anaerobic acetate oxidation via the TCA cycle, and similarity to homologs in *Shewanella oneidensis* MR-1 (if present).

**Table S3.** *Shewanella algae* MN-01 genes putatively involved in anaerobic acetate oxidation via the Wood-Ljungdahl pathway, and similarity to homologs in *Shewanella oneidensis* MR-1 (if present).

**Table S4.** *Shewanella algae* MN-01 genes encoding flavin-based electron bifurcation-related proteins, and similarity to homologs in *Shewanella oneidensis* MR-1 (if present).